

## Hydrogen Generation Catalyzed by Fluorinated Diglyoxime–Iron Complexes at Low Overpotentials

Michael J. Rose, Harry B. Gray, and Jay R. Winkler\*

Beckman Institute, California Institute of Technology, Pasadena, California 91125, United States

## S Supporting Information

**ABSTRACT:**  $\text{Fe}^{\text{II}}$  complexes containing the fluorinated ligand 1,2-bis(perfluorophenyl)ethane-1,2-dionedioxiime ( $\text{dAr}^{\text{F}}\text{gH}_2$ ; H = dissociable proton) exhibit relatively positive  $\text{Fe}^{\text{II/I}}$  reduction potentials. The air-stable difluoroborated species  $[(\text{dAr}^{\text{F}}\text{gBF}_2)_2\text{Fe}(\text{py})_2]$  (**2**) electrocatalyzes  $\text{H}_2$  generation at  $-0.9$  V vs SCE with  $i_{\text{cat}}/i_{\text{p}} \approx 4$ , corresponding to a turnover frequency (TOF) of  $\sim 20$   $\text{s}^{-1}$  [Faradaic yield (FY) =  $82 \pm 13\%$ ]. The corresponding monofluoroborated, proton-bridged complex  $[(\text{dAr}^{\text{F}}\text{g}_2\text{H-BF}_2)\text{Fe}(\text{py})_2]$  (**3**) exhibits an improved TOF of  $\sim 200$   $\text{s}^{-1}$  ( $i_{\text{cat}}/i_{\text{p}} \approx 8$ ; FY =  $68 \pm 14\%$ ) at  $-0.8$  V with an overpotential of 300 mV. Simulations of the electrocatalytic cyclic voltammograms of **2** suggest rate-limiting protonation of an  $\text{Fe}^{\text{II}}$  intermediate ( $k_{\text{RLS}} \approx 200$   $\text{M}^{-1} \text{s}^{-1}$ ) that undergoes hydride protonation to form  $\text{H}_2$ . Complex **3** likely reacts via protonation of an  $\text{Fe}^{\text{I}}$  intermediate that subsequently forms  $\text{H}_2$  via a bimetallic mechanism ( $k_{\text{RLS}} \approx 2000$   $\text{M}^{-1} \text{s}^{-1}$ ). **3** catalyzes production at relatively positive potentials compared with other iron complexes.

The production of  $\text{H}_2$  from proton sources is a major goal of contemporary energy science.<sup>1</sup> Pt is the most efficient catalyst, but its low abundance and high cost prohibit its widespread use. Researchers have investigated alternative alloys,<sup>2</sup> materials,<sup>3</sup> and molecules<sup>4–7</sup> to achieve  $\text{H}_2$  generation using more abundant elements. In seminal work, DuBois and co-workers reported that Ni and Co phosphines exhibit high turnover frequencies (TOFs) of  $10^3$ – $10^5$   $\text{s}^{-1}$  at low overpotentials (50–400 mV).<sup>6</sup> Co diglyoximes<sup>7</sup> also operate at low overpotentials with high rates,<sup>4,5</sup> and considerable effort has been directed toward elucidating the mechanisms employed by these catalysts.<sup>8</sup> Peters and co-workers<sup>4</sup> and Fontecave and Artero<sup>5</sup> have established some of the factors that facilitate  $\text{H}_2$  catalysis in tetraamine systems, such as a diglyoximate proton bridge.<sup>5</sup> More recently, polypyridine Co complexes reported by Chang<sup>9</sup> as well as our group<sup>10</sup> have been shown to catalyze  $\text{H}_2$  evolution from aqueous systems. Although both Co and Ni are more abundant than Pt, a more attractive candidate for the catalytic metal center is Fe, the most abundant transition metal.

Early work by Saveant on an Fe porphyrin,  $[(\text{TPP})\text{Fe}(\text{Cl})]$  (TPP = tetraphenylporphyrin), showed that  $\text{H}_2$  could be produced at very negative  $\text{Fe}^{\text{II/I}}$  potentials (below  $-1.5$  V vs SCE)<sup>11a</sup> with reasonable catalytic rates (Table 1). More recently, Ott and co-workers reported that mononuclear  $[(o\text{-ndt})\text{Fe}(\text{PMe}_3)_2(\text{CO})_2]$  ( $o\text{-ndt}$  =  $o$ -naphthalenedithiolate) also catalyzes  $\text{H}_2$  evolution at similar potentials.<sup>12</sup> Biomimetic diiron

Table 1. Reported Fe Complexes for Electrocatalytic  $\text{H}_2$  Production<sup>a</sup>

catalyst	peak $E_{\text{cat}}$	$i_{\text{cat}}/i_{\text{p}}$	ref
$[(\text{dAr}^{\text{F}}\text{g}_2\text{H-BF}_2)\text{Fe}(\text{py})_2]$ ( <b>3</b> )	$-0.8$	8	this work
$[(\text{dAr}^{\text{F}}\text{gBF}_2)_2\text{Fe}(\text{py})_2]$ ( <b>2</b> )	$-0.9$	4	this work
$[(\text{TPP})\text{Fe}(\text{Cl})]$	$-1.6$	$\sim 10$	11a
$[(o\text{-ndt})\text{Fe}(\text{PMe}_3)_2(\text{CO})_2]$	$-1.4$	$\sim 10$	12a
$\mu\text{-pdt}[\text{Fe}(\text{CO})_3][\text{Fe}(\text{CO})_2\text{IMes}]$	$-1.9$	$\sim 4$	13a
$[\text{Fe}_2(\text{S}_2\text{C}_3\text{H}_6)(\text{CO})_3(\text{dpv})\text{NO}]^+$	$-0.8$	$\sim 2$	14a
$\mu\text{-(SC}_6\text{H}_4\text{-2-(CO)S)[Fe}_2(\text{CO})_6]$	$-0.9$	$< 2$	19
$(\mu\text{-pdt})[\text{Fe}_2(\text{CO})_5\text{PPyr}_3]$	$-1.3$	$< 2$	20
$[(\text{P}^{\text{Ph}}_2\text{N}^{\text{Ph}}_2)\text{Ni}]^{2+}$	$-0.4$	$\sim 20$	6e
$[(\text{dmgBF}_2)_2\text{Co}(\text{MeCN})_2]$	$-0.65$	$\sim 40$	4a
$[(\text{P}^{\text{Ph}}_2\text{N}^{\text{Ph}}_2)\text{Ni}]^{2+}$	$-0.8$	38	6a

<sup>a</sup> Potentials are in V vs SCE; peak  $E_{\text{cat}}$  and  $i_{\text{cat}}/i_{\text{p}}$  are for a scan rate of 100 mV/s.

systems pioneered by Darensbourg,<sup>13</sup> Rauchfuss,<sup>14</sup> and others<sup>15–17</sup> electrocatalyze  $\text{H}_2$  production at potentials in the range  $-1$  to  $-2$  V vs SCE. For example,  $(\mu\text{-S}(\text{CH}_2)_3\text{S})[\text{Fe}(\text{CO})_3][\text{Fe}(\text{CO})_2\text{IMes}]$  [IMes = 1,3-bis(2,4,6-trimethylphenyl)imidazol-2-ylidene] catalyzes  $\text{H}_2$  generation near  $-2$  V vs SCE;<sup>13</sup> the nitrosylated complex  $[\text{Fe}_2(\text{S}_2\text{C}_3\text{H}_6)(\text{CO})_3(\text{dppv})\text{(NO)}]^+$  [dppv = *cis*-1,2-bis(diphenylphosphino)ethylene], which possesses an  $\text{Fe}^{\text{II/I}}$  couple slightly positive of  $-1$  V vs SCE, shows limited catalytic activity.<sup>14</sup> Lichtenberger and co-workers have summarized the functional [Fe–Fe] models,<sup>18</sup> including contributions from their laboratory. In separate work, Sun and Peng reported that complexes with more weakly donating dithiolates<sup>19</sup> in  $(\mu\text{-SC}_6\text{H}_4\text{-2-(CO)S-}\mu)[\text{Fe}_2(\text{CO})_6]$  or ancillary phosphines<sup>20</sup> in  $(\mu\text{-pdt})[\text{Fe}_2(\text{CO})_5\text{PPyr}_3]$  (pdt = propanedithiolate; PPyr = tripyrrolylphosphine) exhibit  $\text{Fe}^{\text{II/I}}$  couples closer to  $-1$  V vs SCE but have limited catalytic activity [peak catalytic current/noncatalytic current ratio ( $i_{\text{cat}}/i_{\text{p}}$ )  $< 2$ ]. Overall, because of the inherent limitations of the  $[\mu\text{-S}_2\text{-Fe}_2]$  scaffold and negative  $\text{Fe}^{\text{II/I}}$  reduction potentials, there is no example of a biomimetic Fe catalyst that operates at reasonable potentials ( $E_{\text{cat}} > -1$  V vs SCE) and exhibits high  $i_{\text{cat}}/i_{\text{p}}$  values.

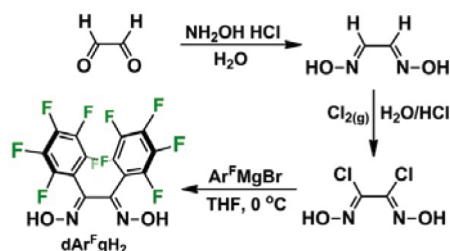
Fe analogues of cobaloximes  $[(\text{dRg})\text{Fe}(\text{L})_2]$ ; dRg = disubstituted glyoxime; R =  $\text{CH}_3$ ,  $\text{C}_6\text{H}_5$ ; L = MeCN, pyridine, imidazole) have been reported by Stynes,<sup>21</sup> but very negative  $[(\text{L})\text{Fe}]/[(\text{L})\text{Fe}]^-$  reduction potentials ( $-1.8$  V vs SCE) render them unsuitable for  $\text{H}_2$  catalysis. We reasoned that dramatic modifications of the dianionic ligand could mitigate

Received: January 17, 2012

such negative reduction potentials. Here we report the syntheses of fluorinated Fe complexes with  $[(L)Fe]/[(L)Fe]^-$  reduction potentials more positive than  $-1$  V vs SCE that catalyze the production of  $H_2$  from trifluoroacetic acid (TFA) in  $CH_2Cl_2$  (or MeCN) solution.

Reaction of aqueous glyoxal with  $NH_2OH \cdot HCl$  precipitates glyoxime, which can then react with  $Cl_2(g)$  in aqueous HCl to afford dichloroglyoxime ( $dCl_2gH_2$ ) in moderate yield (40% for two steps; Scheme 1). Treatment of  $dCl_2gH_2$  with the Grignard reagent derived from pentafluorobromobenzene ( $Ar^F MgBr$ , generated with 1 equiv of  $iPrMgBr$ ) affords  $dAr^FgH_2$  in good yield (65%).

Scheme 1. Synthesis of  $dAr^FgH_2$



Metalation of  $dAr^FgH_2$  (2 equiv) with  $Fe^{II}$  acetate in MeCN containing 5 equiv of pyridine (py) proceeded smoothly to afford gram quantities of an air-stable violet solid,  $[(dAr^FgH)_2Fe(py)_2]$  (**1**), in good yield (73%); recrystallization from  $CHCl_3$ /pentane afforded X-ray-quality crystals ( $wR_2 = 0.0416$ ,  $P2_1/c$ ). In the structure of **1** (Figure 1, top), the Fe

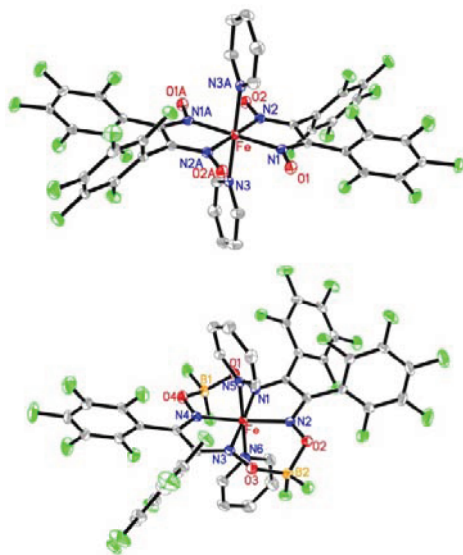


Figure 1. ORTEP diagrams of (top) **1** and (bottom) **2** (50% ellipsoids; H atoms omitted for clarity).

center is in a plane of symmetry, with  $Fe-N_{gly}$  distances [1.896(1) and 1.901(1) Å] significantly shorter than those in the related nonfluorinated complex  $[(dpgH)_2Fe(3-MePy)_2]$  (1.976 Å).<sup>22</sup> The pyridines [ $Fe-N_{py} = 2.001(1)$  Å] are in a parallel orientation, similar to those in  $[(dpgH)Fe(3-MePy)_2]$ .<sup>22</sup> The IR spectrum of **1** exhibits  $\nu_{CN}$  at 1524  $cm^{-1}$ , which is red-shifted relative to free  $dAr^FgH_2$  ( $\nu_{CN} = 1658$   $cm^{-1}$ ). Solutions of **1** in  $CD_3CN$  or  $CD_2Cl_2$  exhibit sharp  $^1H$  and  $^{19}F$  NMR peaks in the diamagnetic region, consistent with

a low-spin  $Fe^{II}$  ground state. Red-violet solutions of **1** in  $CH_2Cl_2$  exhibit an intense feature at 560 nm [ $\epsilon = 11\,200\,M^{-1}\,cm^{-1}$ ; Figure S1 in the Supporting Information (SI)], which we assign to a metal-to-ligand charge transfer (MLCT). The cyclic voltammogram (CV) of **1** in  $CH_2Cl_2$  exhibits a reversible  $Fe^{III/II}$  couple at +0.83 V vs SCE and two irreversible reductions at  $-1.57$  and  $-1.87$  V vs SCE (Figure S2). Such negative potentials prompted further modification to bring the reduction potential into a reasonable range for  $H_2$  electrocatalysis.

Reaction of **1** with 6 equiv of  $BF_3 \cdot Et_2O$  in 1:3 MeCN/ $Et_2O$  followed by workup in  $CHCl_3$ /py (10:1) afforded a bluish-violet solution. Vapor diffusion of pentane crystallized the difluoroborated complex  $[(dAr^FgBF_2)_2Fe(py)_2]$  (**2**) as violet needles ( $wR_2 = 0.0425$ ,  $P\bar{1}$ ). The crystal structure of **2** (Figure 1, bottom) reveals fluoroboration of both glyoxime moieties, resulting in macrocyclic chelation of the Fe center. The  $Fe-N_{gly}$  bond distances [1.881(1) and 1.884(1) Å] are slightly shorter than those in **1**, likely as a result of macrocyclic encapsulation; they are also shorter than those in the closely related complex  $[(dmgBF_2)_2Fe(py)_2]$  [ $Fe-N_{gly} = 1.905(5)$ ].<sup>23</sup> The axial pyridines in **2** adopt a perpendicular orientation, as found in  $[(dmgBF_2)_2Fe(py)_2]$ , with distinct axial  $Fe-N_{py}$  distances [1.998(1) vs 2.042(1) Å] due to steric effects associated with the tilting of the two  $BF_2$  groups downward toward one py moiety.

In the solid state,  $\nu_{CN}$  of **2** is blue-shifted to 1558  $cm^{-1}$  due to the presence of the electron-withdrawing  $BF_2$  groups ( $\nu_{BF} = 1100\,cm^{-1}$ ). Violet solutions of **2** exhibit a red-shifted MLCT band at 570 nm ( $\epsilon = 14\,700\,M^{-1}\,cm^{-1}$ ,  $CH_2Cl_2$ ; Figure S1) and sharp  $^1H$  and  $^{19}F$  NMR peaks in the diamagnetic region ( $CDCl_3$  or  $CD_3CN$ ). Solutions of **2** are air-stable, and electrochemical experiments revealed no  $Fe^{III/II}$  couple up to +1.5 V vs SCE, indicating a highly stabilized  $Fe^{II}$  center. Complex **2** exhibits an irreversible reduction at  $-0.71$  V, followed by a reversible redox couple at  $-0.94$  V (Figure S3). The oxidation wave near +0.5 V was observed only after proceeding through the one-electron reduction, and all three features originate from solution processes, as determined by the scan rate ( $\nu$ ) dependence (linear  $i_p$  vs  $\sqrt{\nu}$  plot; Figure S4). The CV of **2** could be simulated (DigiElch) by a model that included rapid loss of pyridine ( $K_{eq} = 1 \times 10^7\,M^{-1}$  and  $k_{off} = 500\,s^{-1}$ ) upon reduction of  $Fe^{II}$  to  $Fe^I$  (Scheme S1A in the SI).

To test the catalytic ability of **2**, we obtained CVs at different TFA concentrations. Figure 2 shows a systematic increase in  $i_{cat}$  observed near  $-0.9$  V with increasing acid concentration from 0.1 to 50 mM (Figure S5;  $[2] = 0.5$  mM). The resulting  $i_{cat}/i_p$  value of  $\sim 4$  is higher than that for any reported diiron model complex at equivalent potentials, such as  $[Fe_2(S_2C_3H_6)(CO)_3(dppv)(NO)]^+$  or  $(\mu-SC_6H_4-2-(CO)S-\mu)[Fe_2(CO)_6]$  (both  $i_{cat}/i_p < 2$ ).<sup>14,19</sup> The  $i_{cat}/i_p$  versus [TFA] plots for **2** (low [TFA], linear region) as a function of  $\nu$  (Figure S6) gave a TOF lower limit of  $\sim 25\,s^{-1}$ . The  $i_{cat}/i_p$  value exhibited by **2** is, however, lower than those of some molecular Ni/Co systems in organic solvents:  $[(dmgBF_2)_2Co(MeCN)_2]$  ( $i_{cat}/i_p \approx 30$ );  $[(PPh_2NPh)_2Ni]^{2+}$  (**38**);  $[(P^tBu_2N^Ph)_2Co(MeCN)_3]^{2+}$  (**40**).<sup>4,6</sup>

CVs in MeCN (where  $E_{TFA}^o = -0.51$  V vs SCE and  $pK_a = 12.0$ ; Figures S7 top, S12, and S14)<sup>24</sup> gave nearly identical  $E_{cat}$  and  $i_{cat}/i_p$  values, suggesting an overpotential of 400 mV for **2**. Bulk electrolysis of **2** (at  $-0.95$  V vs SCE) with 30 mM TFA resulted in a relatively linear charge-pass plot (Figure 2 inset) over the course of the first hour (2.6 mol of  $H_2$  mol $^{-1}$  h $^{-1}$ ; 90% activity retained; 30% activity at 3 h), with an  $82 \pm 13\%$  Faradaic yield (FY) of  $H_2$  production. We also simulated the

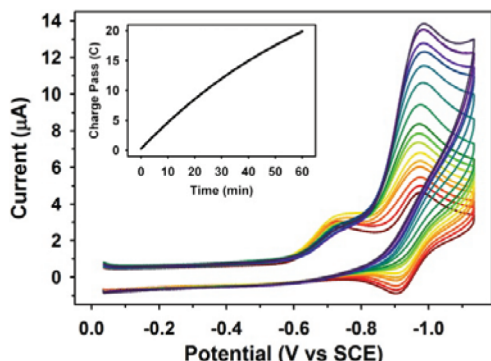


**Figure 2.** CVs for **2** in  $\text{CH}_2\text{Cl}_2$  with increasing [TFA]. Experimental parameters: 0.5 mM **2**, 0–45 mM TFA; 100 mV/s, 0.1 M  $\text{NBu}_4\text{ClO}_4$ ; glassy carbon (GC) working electrode (WE), Ag/AgCl reference electrode (RE), Pt counter electrode (CE). Inset: Charge pass for bulk electrolysis of **2** in MeCN (30 mM TFA).

catalytic CVs of **2** (DigiElch; Scheme S1B and Figure S8). As the catalytic intermediate is a two-electron-reduced complex (putative  $\text{Fe}^{0+}$ ), the data are consistent with a model involving slow protonation of  $\text{Fe}^{0+}$  to form  $\text{Fe}^{\text{II}}\text{--H}$  ( $k_{\text{RLS}} \approx 200 \text{ M}^{-1} \text{ s}^{-1}$ ) followed by rapid protonation of the hydride to form  $\text{H}_2$  and  $\text{Fe}^{\text{II}}$ . A similar mechanism has been invoked in the  $\text{Co}\text{--dmgBF}_2$  system at high acid concentrations.<sup>8</sup> Neither experimental nor simulated plots of  $k_{\text{obs}}$  versus [TFA] (Figure S13) displayed a simple first- or second-order dependence on [TFA], suggesting that  $k_{\text{obs}}$  is a composite of elementary rate constants. Simulations suggested that the acid-independent region (high [TFA]) is not rate-limited by dissociation of py upon reduction of **2**.

During the course of our synthetic work, we isolated an intermediate in the fluoroboration reaction that proved to be an asymmetric complex (Figure 3). This reaction, in which only

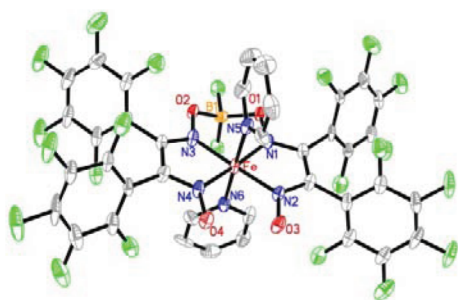


**Figure 3.** ORTEP diagram of **3** (50% ellipsoids; H atoms omitted for clarity).

one side of the diglyoxime complex underwent fluoroboration (4 equiv of  $\text{BF}_3\cdot\text{Et}_2\text{O}$ , 2 h, 1:3 MeCN/ $\text{Et}_2\text{O}$ ), afforded violet crystals of  $[(\text{dAr}^{\text{F}}\text{g}_2\text{H}\text{--BF}_2)\text{Fe}(\text{py})_2]$  (**3**) ( $w_R = 0.067$ ,  $P2_1/c$ ), wherein the proton bridge between O3 and O4 is retained. The bond distances and angles about the Fe center and the spectroscopic properties of **3** (diamagnetic  $^1\text{H}$  and  $^{19}\text{F}$  NMR;  $\lambda_{\text{max}} = 565 \text{ nm}$ ,  $\epsilon = 9780 \text{ M}^{-1} \text{ cm}^{-1}$ ;  $\nu_{\text{CN}} = 1529 \text{ cm}^{-1}$ ) are similar to those of **2**.

Asymmetric fluoroborated complexes are exceedingly rare,<sup>25</sup> but **3** is isolable because of the low reactivity due to the presence of the four  $\text{Ar}^{\text{F}}$  groups. Fontecave and Artero noted the importance of maintaining a proton bridge in  $[(\text{DO})\text{--}(\text{DOH})^{\text{Pr}}\text{Co}(\text{Br})_2]$ , [DO = *N,N*-propanediylbis(2,3-butadiene-

2-imine-3-oxime)] versus the corresponding complex  $[(\text{DO})_2\text{BF}_2]^{\text{Pr}}\text{Co}(\text{Br})_2]$  that does not have  $\text{--OH}$  groups proximal to the metal center.<sup>5</sup> Additionally, DuBois and co-workers emphasized the value of a proton relay in their investigation of complexes containing PNP, P2N2, and P2N ligands.<sup>6</sup>

The CV of **3** (Figure 4, dark-red line) exhibits reduction waves at  $-0.93$  and  $-1.14 \text{ V}$  vs SCE (a pattern similar to **2**),

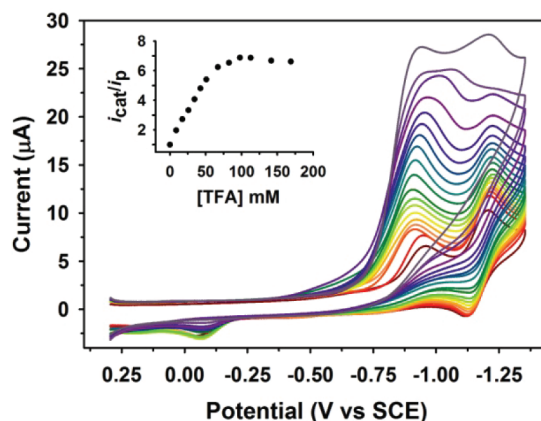


**Figure 4.** CVs of **3** in  $\text{CH}_2\text{Cl}_2$  solution with increasing [TFA]. Inset: Dependence of  $i_{\text{cat}}/i_p$  on [TFA]. Experimental parameters: 0.5 mM **3**, 0–170 mM TFA; 100 mV/s, 0.1 M  $\text{NBu}_4\text{ClO}_4$ ; GC WE, Ag/AgCl RE, Pt CE.

with the latter being reversible ( $E_{1/2} = -1.08 \text{ V}$ ; Scheme S2A). CVs in the presence of increasing [TFA] indicate  $\text{H}_2$  generation, with catalytic onset coinciding with the first reduction wave ( $-0.9 \text{ V}$ ). At higher [TFA] ( $>75 \text{ mM}$ ), catalysis was also observed at the second reduction wave, contributing an additional  $\sim 10\%$  to  $i_{\text{cat}}$ . The operating potential for **3** in the presence of TFA ( $-0.8 \text{ V}$ ) is shifted 100 mV positive versus the  $\text{Fe}^{\text{II/I}}$  potential in the absence of acid, possibly because of substitution of py (protonated by TFA; see Scheme S2B). Catalyst **3** remains active at higher acid concentrations ( $>150 \text{ mM}$ ) than for **2** (50 mM) (Figure 4 inset and Figure S11). The  $i_{\text{cat}}/i_p$  value ( $\sim 8$ ,  $\text{FY} = 68 \pm 14\%$ ,  $2.9 \text{ mol of H}_2 \text{ mol}^{-1} \text{ h}^{-1}$  for the first hour) is twice that for **2** ( $i_{\text{cat}}/i_p = 4$ ) and roughly an order of magnitude greater than those of other Fe catalysts that operate at similar potentials. Indeed, **3** retains a greater extent of activity than **2** after 1 h (99 vs 90%; Figure S9) and after 3 h (70 vs 30%). Indeed, the only comparable  $i_{\text{cat}}/i_p$  values are exhibited by  $[(\text{TPP})\text{Fe}(\text{Cl})]$  and  $[(o\text{--ndt})\text{Fe}(\text{PMe}_3)_2(\text{CO})_2]$ ,<sup>11,12</sup> both of which operate at potentials  $\sim 500 \text{ mV}$  more negative than **2** or **3**. The  $E_{\text{cat}}$  exhibited by **3** ( $-0.8 \text{ V}$ ) suggests that it catalyzes  $\text{H}_2$  production using TFA at an overpotential of only 300 mV, which is 100 mV less than that of  $[(\text{dmgBF}_2)_2\text{Co}(\text{MeCN})_2]$  ( $E_{\text{cat}} = -0.65 \text{ V}$ ) with  $\text{TosH}$  ( $E_{\text{TosH}}^{\text{ox}} = -0.25 \text{ V}$ ).<sup>24</sup>

Simulations of the electrocatalytic CVs for **3** indicate an  $\text{Fe}^{\text{I}}$  species to be the primary active intermediate (Scheme S2B), consistent with the previously proposed bimetallic mechanism<sup>4</sup> (for  $\text{Co}^{\text{I}}$ ) that relies on rate-limiting oxidative protonation of  $\text{Fe}^{\text{I}}$  to form an  $\text{Fe}^{\text{III}}\text{--H}$  intermediate, which rapidly decays through a bimetallic pathway to form  $\text{H}_2$  and the  $\text{Fe}^{\text{II}}$  starting material. Although we could not simulate the CVs assuming a monometallic mechanism, we cannot rule out this possibility.<sup>11d</sup> Our simulation (Figure S10) suggests  $k_{\text{RLS}} \approx 2000 \text{ M}^{-1} \text{ s}^{-1}$  and a corresponding TOF of  $200 \text{ s}^{-1}$ ; these values represent



a 10-fold enhancement in catalysis versus **2** ( $k_{\text{RLS}} \approx 200 \text{ M}^{-1} \text{ s}^{-1}$ , TOF =  $20 \text{ s}^{-1}$ ). In this respect, catalysts **2** ( $\text{Fe}^{0+}$  active species) and **3** ( $\text{Fe}^{\text{I}}$  active species) represent a unique opportunity to explore differing mechanisms within the same ligand/metal system at similar driving forces.

The lower activity of dAr<sup>F</sup>-derived Fe catalysts versus existing Co/Ni complexes may be substantially offset by the greater abundance and lower cost of iron. We are now exploring other electronic and structural modifications to the {dAr<sup>F</sup>gX} (X = H, BF<sub>2</sub>, BR<sub>2</sub>) ligand system in attempts to achieve lower overpotentials and higher catalytic efficiencies.

## ■ ASSOCIATED CONTENT

### ● Supporting Information

CIF for **1–3**; additional spectra, experimental and simulated CVs, and resulting analyses; and supporting reaction schemes. This material is available free of charge via the Internet at <http://pubs.acs.org>.

## ■ AUTHOR INFORMATION

### Corresponding Author

winklerj@caltech.edu

### Notes

The authors declare no competing financial interest.

## ■ ACKNOWLEDGMENTS

This work was supported by the NSF CCI Solar Fuels Program (CHE-0802907). M.J.R. was supported by an NSF ACC-F Fellowship (CHE-1042009). The Bruker APEXII diffractometer was obtained via an NSF CRIF:MU Award (CHE-0639094). We thank Larry Henling and Michael Day for solving the crystal structures.

## ■ REFERENCES

- (1) (a) Walter, M. G.; Warren, E. L.; McKone, J. R.; Boettcher, S. W.; Mi, Q.; Santori, E. A.; Lewis, N. S. *Chem. Rev.* **2010**, *110*, 6446. (b) Lewis, N. S.; Nocera, D. G. *Proc. Natl. Acad. Sci. U.S.A.* **2006**, *103*, 15729. (c) Gray, H. B. *Nat. Chem.* **2009**, *1*, 7.
- (2) Trasatti, S. *Adv. Electrochem. Sci. Eng.* **1992**, *2*, 1.
- (3) (a) Woodhouse, M.; Parkinson, B. A. *Chem. Soc. Rev.* **2009**, *38*, 197. (b) Jaramillo, T. F.; Jørgenson, K. P.; Bonde, J.; Nielson, J. H.; Horch, S.; Chorkendorff, I. *Science* **2007**, *317*, 100. (c) Merki, D.; Fierro, S.; Vrubel, H.; Hu, X. *Chem. Sci.* **2011**, *2*, 1262.
- (4) (a) Hu, X.; Brunswig, B. S.; Peters, J. C. *J. Am. Chem. Soc.* **2007**, *129*, 8988. (b) Dempsey, J. L.; Brunswig, B. S.; Winkler, J. R.; Gray, H. B. *Acc. Chem. Res.* **2009**, *42*, 1995. (c) Hu, X.; Cossairt, B. M.; Brunswig, B. S.; Lewis, N. S.; Peters, J. C. *Chem. Commun.* **2005**, 4723.
- (5) (a) Baffert, C.; Artero, V.; Fontecave, M. *Inorg. Chem.* **2007**, *46*, 1817. (b) Razavet, M.; Artero, V.; Fontecave, M. *Inorg. Chem.* **2005**, *44*, 4786. (c) Fourmond, V.; Jacques, P.-A.; Fontecave, M.; Artero, V. *Inorg. Chem.* **2010**, *49*, 10338. (d) Jacques, P.-A.; Artero, V.; Pécaut, J.; Fontecave, M. *Proc. Natl. Acad. Sci. U.S.A.* **2009**, *106*, 20627.
- (6) (a) Helm, M. L.; Stewart, M. P.; Bullock, R. M.; Rakowski-DuBois, M.; DuBois, D. L. *Science* **2011**, *333*, 863. (b) Kilgore, U. J.; Roberts, J. A. S.; Pool, D. H.; Appel, A. M.; Stewart, M. P.; Rakowski-DuBois, M.; Dougherty, W. G.; Kassel, W. S.; Bullock, R. M.; DuBois, D. L. *J. Am. Chem. Soc.* **2011**, *133*, 5861. (c) Wiedner, E. S.; Yang, J. Y.; Dougherty, W. G.; Kassel, W. S.; Bullock, R. M.; Rakowski-DuBois, M.; DuBois, D. L. *Organometallics* **2010**, *29*, 5390. (d) Rakowski-DuBois, M.; DuBois, D. L. *Acc. Chem. Res.* **2009**, *42*, 1974. (e) Wilson, A. D.; Newell, R. H.; McNevin, M. J.; Muckerman, J. T.; Rakowski-DuBois, M.; Dubois, D. L. *J. Am. Chem. Soc.* **2006**, *128*, 358.
- (7) (a) Schrauzer, G. N.; Windgassen, R. J. *J. Am. Chem. Soc.* **1966**, *88*, 3738. (b) Connolly, P.; Espenson, J. H. *Inorg. Chem.* **1986**, *25*, 2684.
- (8) (a) Dempsey, J. R.; Winkler, J. R.; Gray, H. B. *J. Am. Chem. Soc.* **2010**, *132*, 1060. (b) Dempsey, J. R.; Winkler, J. R.; Gray, H. B. *J. Am. Chem. Soc.* **2011**, *132*, 16774.
- (9) (a) Sun, Y.; Bigi, J. P.; Piro, N. A.; Tang, M. L.; Long, J. R.; Chang, C. J. *J. Am. Chem. Soc.* **2011**, *133*, 9212. (b) Bigi, J. P.; Hanna, T. E.; Harman, W. H.; Chang, A.; Chang, C. J. *Chem. Commun.* **2010**, *46*, 958.
- (10) Stubbert, B.; Peters, J. C.; Gray, H. B. *J. Am. Chem. Soc.* **2011**, *133*, 18070.
- (11) (a) Bhugun, I.; Lexa, D.; Saveant, J.-M. *J. Am. Chem. Soc.* **1996**, *118*, 3982. (b) Saveant, J.-M. *Chem. Rev.* **2008**, *108*, 2348. (c) Costentin, C.; Robert, M.; Saveant, J.-M. *Acc. Chem. Res.* **2010**, *43*, 1019. (d) Andrieux, C. P.; Blocman, C.; Dumascouchiat, J. M.; Mhalla, F.; Saveant, J.-M. *J. Electroanal. Chem.* **1980**, *113*, 19.
- (12) (a) Kaur-Ghumaan, S.; Schwartz, L.; Lomoth, R.; Stein, M.; Ott, S. *Angew. Chem., Int. Ed.* **2010**, *49*, 8033. (b) Schwartz, L.; Singh, P. S.; Eriksson, L.; Lomoth, R.; Ott, S. C. R. *Chim.* **2008**, *11*, 875.
- (13) (a) Tye, J. W.; Lee, J.; Wang, H.-W.; Mejia-Rodriguez, R.; Reibenspies, J. H.; Hall, M. B.; Darensbourg, M. Y. *Inorg. Chem.* **2005**, *44*, 5550. (b) Georgakaki, I. P.; Thomson, L. M.; Lyon, E. J.; Hall, M. B.; Darensbourg, M. Y. *Coord. Chem. Rev.* **2003**, *238–239*, 255. (c) Darensbourg, M. Y.; Lyon, E. J.; Smee, J. J. *Coord. Chem. Rev.* **2000**, *206*, 533.
- (14) (a) Olsen, M. T.; Justice, A. K.; Gloaguen, F.; Rauchfuss, T. B.; Wilson, S. R. *Inorg. Chem.* **2008**, *47*, 11816. (b) Royer, A. M.; Stagni-Salomone, M.; Rauchfuss, T. B.; Meyer-Klaucke, W. J. *J. Am. Chem. Soc.* **2010**, *132*, 16997.
- (15) Tard, C.; Pickett, C. J. *Chem. Rev.* **2009**, *109*, 2245.
- (16) Fontecilla, J. C.; Ragsdale, S. W. *Adv. Inorg. Chem.* **1999**, *47*, 283.
- (17) Ezzaher, S.; Orain, P.-Y.; Capon, J.-F.; Gloaguen, F.; Pétillon, F. Y.; Roisnel, T.; Schollhammer, P.; Talarmin, J. *Chem. Commun.* **2008**, 2547.
- (18) Felton, G. A. N.; Mebi, C. A.; Petro, B. J.; Vannucci, A. K.; Evans, D. H.; Glass, R. S.; Lichtenberger, D. L. *J. Organomet. Chem.* **2009**, *17*, 2681.
- (19) Wang, Z.; Jiang, W.; Liu, J.; Jiang, W.; Wang, Y.; Åkerman, B.; Sun, L. *J. Organomet. Chem.* **2008**, *693*, 2828.
- (20) Huo, F.; Hou, J.; Chen, G.; Guo, D.; Peng, X. *Eur. J. Inorg. Chem.* **2010**, 3942.
- (21) (a) Thompson, D. W.; Stynes, D. V. *Inorg. Chem.* **1990**, *29*, 3815. (b) Pang, I. W.; Stynes, D. V. *Inorg. Chem.* **1977**, *16*, 590.
- (22) Dvorkin, A. A.; Simonov, Y. A.; Malinovskii, T. I.; Bulgak, I. I.; Batir, D. G. *Proc. Natl. Acad. Sci. USSR* **1977**, *234*, 1372.
- (23) Vernik, I.; Stynes, D. V. *Inorg. Chem.* **1996**, *35*, 6210.
- (24) (a) Felton, G. A. N.; Glass, R. S.; Lichtenberger, D. L.; Evans, D. H. *Inorg. Chem.* **2006**, *45*, 9181. (b) Eckert, F.; Leito, I.; Kaljurand, I.; Kütt, A.; Klamt, A.; Diedenhofen, M. *J. Comput. Chem.* **2008**, *30*, 799.
- (25) Chmielewski, P. J. P.; Warburton, R. P.; Morales, L.; Stephenson, N. A.; Busch, D. H. *J. Coord. Chem.* **1991**, *23*, 91.